IMR Press

Original Research

The pathomechanism of human myxomatous valvular degeneration at the mechanical and cellular level

Chang Hu[1,†], Qian Wang[1,†], Hui Xue[2], Hao Hong[3], Jiawei Shi[3], Nianguo Dong[3,*], Mingkui Zhang[2,*]

[1] *Department of Vascular Surgery, The First Hospital of Tsinghua University, 100016 Beijing, China*

[2] *Department of Cardiac Surgery, The First Hospital of Tsinghua University, 100016 Beijing, China*

[3] *Department of Cardiovascular Surgery, Union Hospital, Tongji Medical College, Huazhong University of Science and Technology, 430022 Wuhan, Hubei, China*

*Correspondence: nianguodonguh@163.com (Nianguo Dong); mingkuizhanghx@163.com (Mingkui Zhang)
† These authors contributed equally.

DOI:10.31083/j.rcm2202059

Submitted: 11 April 2021 Revised: 7 May 2021 Accepted: 11 June 2021 Published: 30 June 2021

The purpose of this study was to explore the pathomechanism of human myxomatous valve degeneration by investigating changes in the phenotype of valvular cells, the metabolism of the extracellular matrix and their mechanical properties. Mitral valve specimens were harvested from patients who had undergone valve replacement, and divided into two groups: patients with a myxomatous mitral valve and a control group. Histological investigation showed that the morphology of the extracellular matrix was looser and less coordinated in myxomatous valves than in controls. α-SMA (α-smooth muscle actin) and Vimentin were positive and DNA (deoxyribonucleic acid) assay of leaflets and expression of SMemb (embryonic smooth muscle myosin heavy chain), MMP-13 (matrix Metalloproteinases-13), MMP-1 mRNA (messenger Ribonucleic Acid) of the myxomatous valves were increased while the hydroxyproline content, expression of TIMP-1 (tissue inhibitor of metalloproteinase-1) mRNA and mechanical properties were decreased compared with controls. Compared to the quiescent interstitial cells in non-myxomatous valves, interstitial cells in myxomatous valves exhibit myofibroblast activation and express excessive levels of matrix metalloproteinases. The balance between MMP/TIMP was disrupted. We conclude that overactivation of VICs (Valvular interstitial cells) and the imbalance of MMP/TIMP could be important features of the pathomechanism of myxomatous mitral valve degeneration.

Keywords

Myxomatous mitral valve; Degeneration; Valvular interstitial cell; Extracellular matrix; Mechanical property

1. Introduction

Due to continuous improvements in global medical care over many decades, the incidence of rheumatic valvular heart disease has been decreasing year by year. In contrast, myxomatous degenerative heart valve disease has gradually become a serious cardiovascular disease that affects the quality of life and life expectancy of the elderly worldwide [1–3]. The exact cause of myxomatous degenerative valve disease is still unknown. At present, research on this disease has focused on morphology, while the study of its pathological mechanism at the mechanical and cellular level has received little attention. The aim of this study was to explore the mechanism of valvular degenerative pathological changes by detecting changes in the phenotype of valvular interstitial cells, extracellular matrix (ECM) metabolism, valve structure, and mechanical properties, and therefore provide a theoretical basis for the prevention and treatment of myxomatous degenerative valve disease in the future.

2. Materials and methods

2.1 Valve acquisition, grouping and processing

A total 26 of mitral valve specimens (anterior leaflet) were selected from patients who underwent valve replacement surgery, which were then divided into two groups: A myxomatous mitral valve group (hereafter referred to as diseased, n = 20, specimens were obtained from patients with myxomatous degenerative mitral valve which could not be reconstructed, 12 males and 8 females aged 70.3 $\pm$ 7.06 years) and a non-myxomatous mitral valve group (hereafter referred to as control, n = 6, specimens were obtained from replaced prolapsed mitral valves where the mitral chordae tendineae had undergone acute mechanical rupture and failed to be reconstructed, with no evidence of pathological change, 4 males and 2 females aged 68.5 $\pm$ 5.89 years). There was no significant difference in gender and age between the two groups ($P > 0.05$). In order to ensure that every specimen of the diseased group represented a myxomatous degenerative valve, the following diseases were excluded: rheumatic heart disease, endocarditis, calcific degeneration as well as any uncertain diagnosis of myxomatous degeneration. Valve specimens of both groups were confirmed by postoperative pathological examination. All analyses were conducted by the pathologist who is an expert in the study of valvular heart diseases and blinded to the study group allocations. The specimens were immediately stored in cold phosphate buffer solution (PBS) solution containing antibiotics (penicillin 100

u/mL, streptomycin 100 u/mL) after harvest, and assays were performed on the same day. All patients involved in this study gave their informed consent. Institutional review board (IRB) approval of our hospital was obtained for this study (IRB file number: 2020-36).

2.2 Detection indicators and methods

2.2.1 Histology

Valve specimens were fixed in 10% neutral formalin, embedded in paraffin, and cut transversely in 5-μm thick sections, which were stained with hematoxylin and eosin for further histological analysis.

2.2.2 Immunofluorescence chemical detection of phenotype of valvular interstitial cells

Serial 5-μm sections of frozen fragments from the valve specimens were transferred to silane-treated microscope slides, fixed in 4% paraformaldehyde for 4 hours and submitted to treatment with 0.1% Triton X-100 for 5 minutes, followed by three washes in PBS. After being blocked with goat serum at room temperature, samples were incubated with α-smooth muscle actin (α-SMA) monoclonal antibodies (human 1 : 100) and Vimentin monoclonal antibodies (human 1 : 100) for one hour at 37 °C. Then slides were washed 3 times in PBS and secondary antibodies labeled by fluorescein isothiocyanate (FITC) (Sigma, USA, 1 : 150) were added. The slides were incubated in a humidity chamber for one hour at 37 °C in the dark and washed three times in PBS each. The tissue-images were observed under inverted fluorescence microscopy for green fluorescence positivity.

2.2.3 DNA content analysis

Excessive water on the surface of fragments from the valve specimens was removed by clean absorbent paper. The specimens were then weighed, ground, and homogenized in PBS, followed by centrifugation (3000 r/min) for 5 minutes. After the addition of 500 μL of RNA lysis buffer and 5 μL of 20 mg/mL proteinase-K, the specimen pellets were incubated for 12 hours in a 37 °C water bath. After incubation, 500 μL of phenol-chloroform-isoamyl alcohol (25 : 24 : 1) was added and the solution was centrifuged (10000 r/min) for 15 minutes. The aqueous phase was transferred to new Eppendorf tubes, 40 μL of 3 mol/L sodium acetate mixed with 1 mL of cold ethanol were added and allowed to stand at –20 °C for 30 minutes, followed by centrifugation (14000 r/min) for 20 minutes. The supernatant was then discarded and the precipitate dried at room temperature for 10 minutes and dissolved in 40 μL of TE solution (PH = 8.0). The DNA quantizer (GeneQuant Pro, Biochrom, England) was used to measure the absorbance at 260 nm, and the DNA content was calculated.

2.2.4 Hydroxyproline content

The surface of the valve specimens was dried with absorbent paper. Specimens were weighed and tested in accordance with the operating instruction of the hydroxyproline reagent cartridge for processing. Elx800uv microplate reader (Bio-Tek, Milton, VT, USA) was used to test the absorbance of samples at 550 nm, and the hydroxyproline content of the samples was calculated.

2.2.5 Mechanical performance test

Valve specimens were cut into 1.5 × 0.5 cm rectangular strips along their long axis and mounted on a AGS-J (SHIMADZU, Tokyo, Japan) universal tensile testing machine with a clamping distance of 8 mm. By applying tension to the valve at a velocity of 5 mm/min at a temperature of 24 °C, the stress-strain curve through the transducer was recorded electronically. The measurements were done in one round (no duplicates, n = 6 in each group). Maximum load, maximum stress, maximum strain, and the elastic modulus were calculated and recorded.

2.2.6 Detection of relative mRNA expression of SMemb, MMP-13, MMP-1 and TIMP-1 by reverse transcription-polymerase chain reaction (RT-PCR)

2.2.6.1 Extraction of the total RNA

Valve fragments were placed in an autoclavable mortar and soaked in DEPC, 1 mL of Trizol was added, the fragments were then ground down and transferred to an Eppendorf tube. After standing at room temperature for 5 minutes, 0.2 mL of chloroform was added to the sample and shaken vigorously for 15 seconds, then placed on ice for 5 minutes. Following centrifugation (14000 r/min) at 4 °C for 15 minutes, the upper aqueous phase was transferred to another Eppendorf tube. 500 μL of isopropanol was added to the sample, mixed and placed on ice for 10 minutes, followed by centrifugation (14000 r/min) at 4 °C for 10 minutes. The supernatant was discarded, and the precipitate was added to 1 mL of pre-cooled 75% ethanol, and after shaking was washed thoroughly. Centrifugation (14000 r/min) was completed at 4 °C for 5 minutes, and the supernatant was discarded. The precipitate was dried at room temperature for 5–10 minutes and dissolved in 20 μL of enzyme-free water, then stored in a –70 °C deep cryogenic refrigerator. A small amount of the above sample was used to detect the optical density (OD) value of total RNA to confirm the concentration and purity of RNA by means of an ultraviolet spectrophotometer (A260/A280). Required OD_{260nm}/OD_{280nm} is 1.8 or more and 2.0% agarose gel electrophoresis showed clear 18 s and 28 s bands, which indicated that RNA had been extracted successfully.

2.2.6.2 Reverse transcription

Reverse transcription was carried out according to the instructions of the reverse transcription kit (Fermentas) and samples after reverse transcription were stored in a –20 °C refrigerator.

2.2.6.3 Amplification of the target gene

Primer designs are shown in Table 1 and the PCR reaction system is shown in Table 2. Conditions for PCR amplification were: an initial denaturation at 95 °C for 5 minutes, denaturation at 94 °C for 45 seconds, annealing temperatures

Table 1. RT-PCR detection of SMemb , MMP-13 , MMP-1 and TIMP-1 primer sequences.

Primers	Sequence	Length (bp)	Product Length (bp)	Annealing temperature
SMemb (human)				
Upper primer	5′-CCGCCCAGAAGAGTGACAATG-3′	21	376	64.2 °C
Down primer	5′-TGGAGTTTACGCCGAGATGC-3′	20		
MMP-13 (human)				
Upper primer	5′-TGGCTGCCTTCCTCTTCT-3′	18	235	49.3 °C
Down primer	5′-TCAAGTTTGCCAGTCACCT-3′	19		
MMP-1 (human)				
Upper primer	5′-GAAGAATGATGGGAGGCAAGT-3′	21	523	57.4 °C
Down primer	5′-ATGAGCCGCAACACGATG-3′	18		
TIMP-1 (human)				
Upper primer	5′-AATTCCGACCTCGTCATCAG-3′	20	195	54.5 °C
Down primer	5′-GTTGTGGGACCTGTGGAAGT-3′	20		
α-tublin (reference gene)				
Upper primer	5′-CTCATCACAGGCAAGGAAGAT-3′	21	410	55 °C
Down primer	5′-TTAAGGTAAGTGTAGGTTGGG-3′	21		

were set according to gene primers (see Table 1), annealing time of 45 seconds, extending at 72 °C for 90 seconds, a total of 33 cycles, second extending at 72 °C for 10 minutes and finally annealed at 4 °C.

Table 2. 50 μL RT-PCR reaction system.

10 × PCRbuffer (Mg^{2+} Plus)* 5 μL
dNTP mixture (2.5 mM each) 4 μL
sense primer (10 pmol/μL) 2 μL
antisense primer (10 pmol/μL) 2 μL
Taq DNA polymerase (5 U/μL) 0.25 μL
dH_2O (RNase-free) 34.75 μL
cDNA 3 μL
total volume 50 μL

*10 × PCRbuffer (Mg^{2+} Plus): Tris-HCL (PH 8.3) 100 mM; KCL 500 mM; $MgCl_2$ 15 mM.

2.2.6.4 Gel electrophoresis

5 μL of final products of the target gene and reference gene were added into new Eppendorf tubes and mixed with 1 μL of 6× loaded buffer. Agarose gel electrophoresis was executed with the stain SYBR Green I and electrophoresis buffer of 0.5× TBE for 30 minutes at 100 volts of constant voltage. Bands were observed under ultraviolet light, and photographs were taken rapidly by the one-time imaging system of Polai. Computer software (Bandscan 5.0) analyzed the ratio of the gray value of the target gene to the gray value of the reference gene, which was the relative content of the target gene.

2.2.7 Statistical analysis

Statistical data are presented as standard deviations from the mean. Unpaired Student *t*-test was used to compare means of two experimental groups, and statistical significance was set at the 0.05 level. Statistical analyses were performed with SPSS ver. 23.0 (SPSS Inc., Chicago, IL, USA).

3. Result

3.1 Histology

Histological examination of non-myxomatous valve leaflets demonstrated that cells were distributed in all three layers, of an integrated and compact three-tier structure (a fibrous layer, a sponge layer, and a ventricular layer) which was interconnected by dense fibrous tissue. The diseased valve leaflets showed a slight increase in number of cells. The three-tier structure was still intact. However, fibrous tissue was loose and disordered, and the sponge layer was deeper with more voids (Fig. 1).

3.2 Immunofluorescence

Immunofluorescence for α-SMA was negative or weakly positive in the control group but positive in the diseased group, while Vimentin staining was positive in both groups (Figs. 2,3).

3.3 DNA content and hydroxyproline content

A comparison between groups showed that the DNA content of the diseased group was higher than that of the control group, and the hydroxyproline content was lower than that of the control group (Table 3).

Table 3. DNA content and hydroxyproline content.

	DNA content (μg/mg)	Hydroxyproline content (μg/mg)
Diseased	0.120 ± 0.009*	4.20 ± 0.33*
Control	0.094 ± 0.010	5.21 ± 0.25

*$P < 0.05$.

3.4 Mechanical performance

Compared with the control group, the maximum load and maximum stress of the diseased group decreased, while the maximum strain and elastic modulus increased (Table 4).

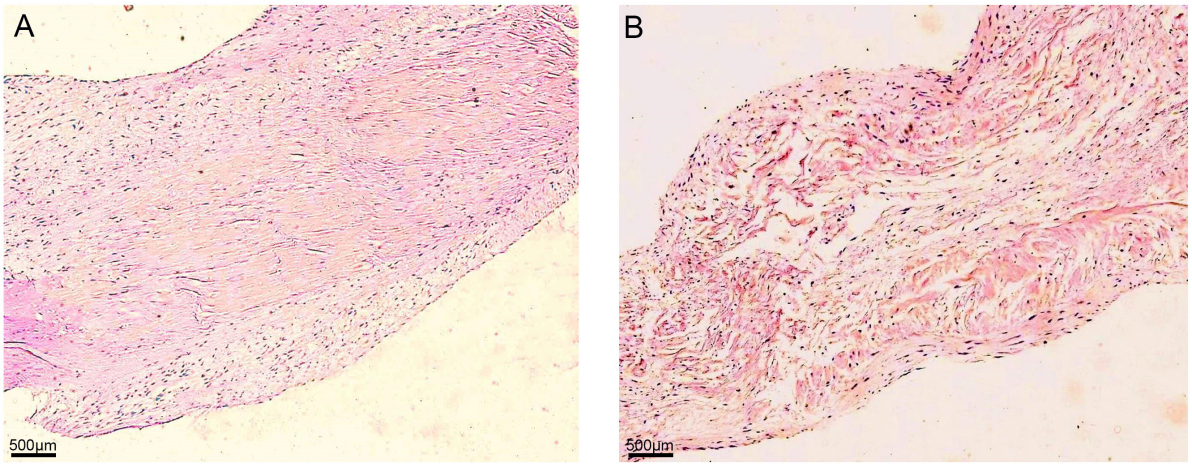

Fig. 1. Histologic examination of valve leaflets. (A) Control group: Cells were distributed in all three layers, of an integrated and compact three-tier structure (fibrous layer, sponge layer, and ventricular layer) which was interconnected by dense fibrous tissue. (B) Diseased group: The number of cells increased slightly. The three-tier structure was still intact, however, fibrous tissue was loose and disordered, and the sponge layer was broader with more voids (A and B: hematoxylin and eosin; original magnification ×20).

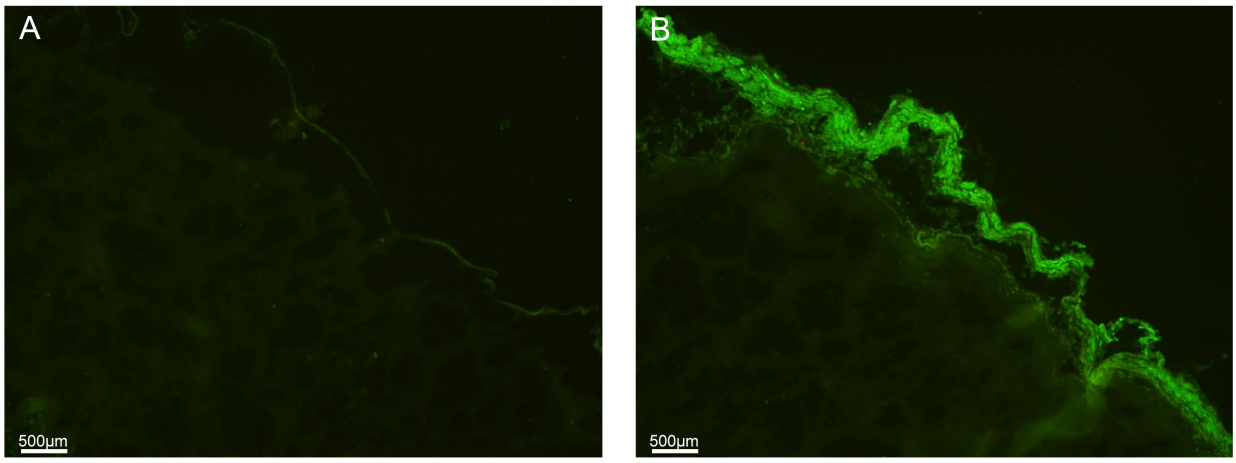

Fig. 2. Immunofluorescent staining for α-SMA in the (A) control group and in the (B) diseased group.

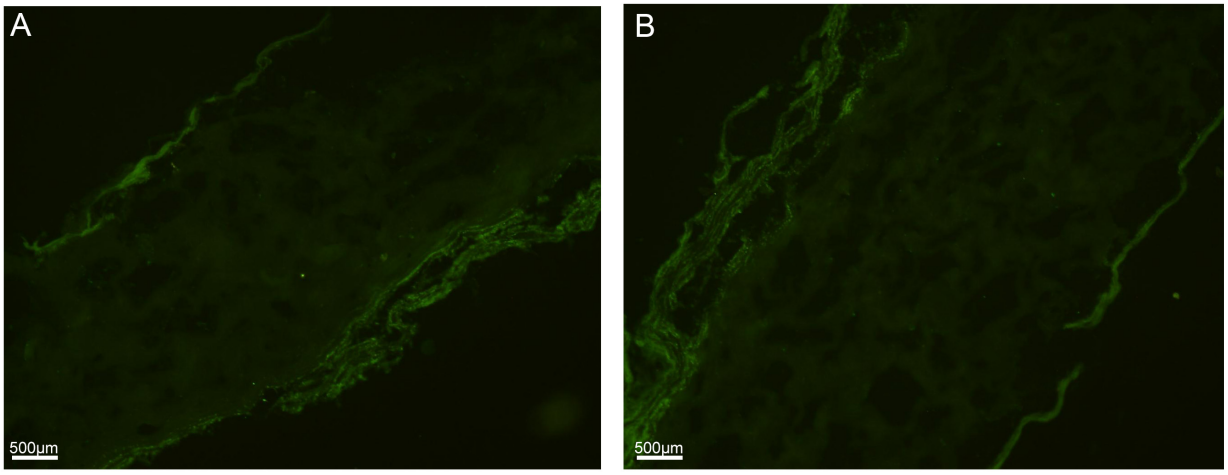

Fig. 3. Immunofluorescent staining for Vimentin in the (A) control group and in the (B) diseased group.

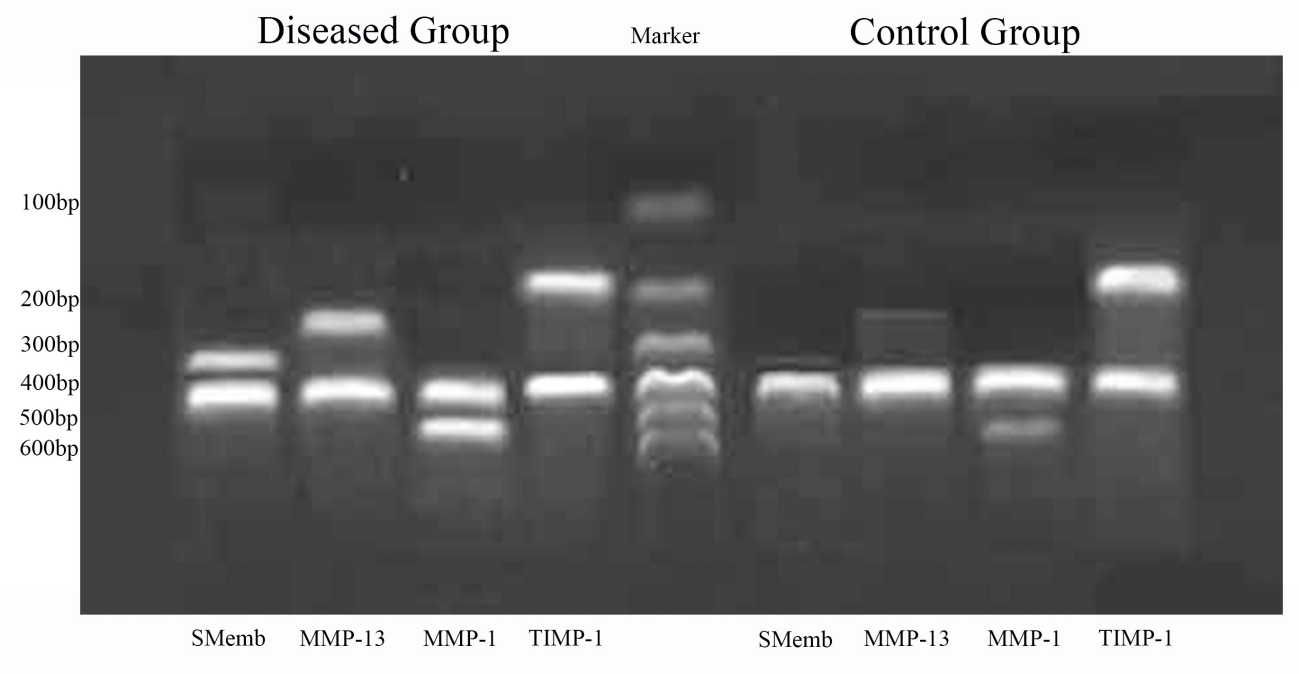

Fig. 4. The gel images of the final products of SMemb, MMP-13, MMP-1 and TIMP-1 mRNA detected by reverse transcription-polymerase chain reaction.

Table 4. Mechanical test results (n = 6).

	Maximum load (N)	Maximum stress (N/mm^2)	Maximum strain (%)	Modulus of elasticity (N/mm^2)
Diseased	$8.01 \pm 0.82^*$	$1.84 \pm 0.21^*$	$63.21 \pm 7.93^*$	$13.43 \pm 1.15^*$
Control	12.92 ± 1.03	2.55 ± 0.37	42.55 ± 4.72	9.49 ± 0.77

$^*P < 0.05$.

3.5 Relative mRNA expression of SMemb, MMP-13, MMP-1 and TIMP-1

The relative content of the target genes—SMemb, MMP-13, MMP-1 and TIMP-1—and the internal reference in the diseased group and the control group are shown in Table 5. The expression of SMemb and MMP-13 are indicators that reflect the cell phenotype; they were hardly detected in the control group, but highly expressed in the diseased group. The expression of MMP-1 and TIMP-1 mRNA reflect general metabolism in the ECM. Compared with the control group, the expression of MMP-1 mRNA in the diseased group was increased, but the expression of TIMP-1 mRNA decreased. The gel images of the final products of SMemb, MMP-13, MMP-1 and TIMP-1 mRNA detected by RT-PCR are shown in Fig. 4.

Table 5. The ratio of the gray value of the target gene and the internal reference in the diseased group and the control group.

	SMemb	MMP-13	MMP-1	TIMP-1
Diseased	$0.55 \pm 0.07^*$	$0.47 \pm 0.06^*$	$0.71 \pm 0.08^*$	$0.70 \pm 0.05^*$
Control	0.03 ± 0.01	0.05 ± 0.01	0.27 ± 0.04	0.88 ± 0.06

$^*P < 0.05$.

4. Discussion

VICs are the predominant cells responsible for the synthesis of extracellular matrix and expression of matrix-degrading enzymes and their inhibitors, which mediate matrix remodeling [4–7]. VICs have been demonstrated to exhibit cell phenotypes in two different states under different conditions, namely fibroblast-like phenotype and myofibroblast-like phenotype [3, 8]. In normal adult valves, VICs mainly manifest as a relatively quiescent fibroblast-like phenotype, while in infancy they exhibit an activated myofibroblast-like phenotype, both of which express Vimentin, but the latter is characterised by expression of α-SMA, SMemb and MMP-13 (collagenase-3) [9, 10]. Some scholars have concluded that activated VICs are also present in pathological cardiac valves, allogeneic valves after transplantation and tissue-engineered valves *in vitro* [11, 12]. The synthesis and secretion of matrix-degrading enzymes and their inhibitors are conducted by the activation of VICs. Matrix metalloproteinases (MMPs) are the most important enzymes that degrade ECM and can degrade almost all constituents of ECM [13, 14]. TIMP is a natural inhibitor of MMPs [15, 16]. As a pair, TIMP and MMP maintain a dynamic balance, and play an important role in regulating the homeostasis of valve ECM [17–19].

Cardiac valves require cells with differing mechanical properties to work together in concert; their strength is closely related to valve structure and chemical composition [20]. The normal heart valve includes a three-tier structure consisting of ventricular layer, spongiosa and fibrous layer, each having a different major constituent (in order: elastin, glycosaminoglycan, and collagen). Different components play differing mechanical roles in the movement of the valve, ensuring normal opening and closing of the valve throughout the cardiac cycle. Elastin permits radial stretch of the leaflets, which allows the valves to extend during diastole and shorten when the heart contracts; glycosaminoglycan shears and cushions impact transmitted from the ventricular layer and the fibrous layer; collagen fibers impart strength and stiffness to the valve, which maintains closure during systole. Clearly, the close relationship of composition-structure-function dictates that changes in the microscopic composition of the valve can lead to changes in the macrostructure, which in turn affects the mechanical properties of the valve and the maintenance of normal function.

The results of this study show that the VICs of non-myxomatous valves demonstrate a relatively static fibroblast-like phenotype, which may be related to the low metabolic rate of relatively normal valve tissue. Positive expression of α-SMA, SMemb and Vimentin was found in the VICs of the diseased group, presenting characteristics of a myofibroblast-like phenotype, which suggests increased metabolic activity with increased DNA content indicating activated VIC proliferation. RT-PCR analysis showed that the expression of MMP-1 mRNA in activated VICs was enhanced, while expression of TIMP-1 mRNA was weakened, suggesting loss of the dynamic balance between MMP/TIMP. We hypothesise that this imbalance could lead to the dysregulation of extracellular matrix metabolism in the diseased valve, which in turn results in a decrease in valve collagen content and structural instability. The hydroxyproline content test showed that the collagen content of the diseased group was decreased, and histological examination confirmed that fibrous tissue of the diseased group was loose and disordered, which supports this hypothesis. Changes in valve composition and tissue structure directly result in changes in the mechanical properties of the valve. The mechanical performance test of this study showed that the maximum load and maximum stress of the diseased valve decreased, while the maximum strain and elastic modulus increased, that is, its strength decreased while its elasticity increased. The former may be caused by an increase in distance between collagen fibers in the diseased group, a more random architectural orientation, and the decrease in fiber per unit area; while the latter is related to the widening of the sponge layer and the increase in water content of the network structure [21]. Changes in the mechanical properties of myxomatous degenerative valves are proposed to cause clinical mitral valve prolapse and lead to valvular insufficiency.

In summary, systemic blood flow impacts the valve leading to degeneration over time, which institutes mechanical stress changes in the valves. VICs are activated and then proliferate, increasing the expression of Vimentin, α-SMA, SMemb, and MMP-13, and activating extracellular matrix remodeling. This system allows the body to adapt to changes in the internal environment. However, in patients with myxomatous degenerative valves, VICs are overactivated and the expression of MMP/TIMP is imbalanced. This causes the dysregulation of ECM metabolism, decreased collagen content of the valve, and a change in structural hierarchy, which ultimately leads to a deterioration in the biomechanical properties of the valve. This study elucidates the profile of human myxomatous valvular degeneration and demonstrates the pathogenesis of myxomatous degenerative valve disease. Further studies should concentrate on whether overactivation of VICs are implicated in other blood fluid rheology related pathologies, such as hypertension and arterial atherosclerosis, in addition to the role of genetic factors. Inhibition of overactivation of VICs might be one way to retard the development and progression of myxomatous valvular degeneration. We hope this work provides a theoretical basis for the prevention and treatment of myxomatous degenerative valve disease in the future.

5. Conclusions

Compared to the quiescent interstitial cells in non-myxomatous valves, interstitial cells in myxomatous valves exhibit myofibroblast activation and express excessive levels of matrix metalloproteinases. The homeostatic balance between MMP/TIMP is disrupted. We conclude that overactivation of VICs and the imbalance of MMP/TIMP could be important features of the pathomechanism of myxomatous mitral valve degeneration.

Author contributions

ND and MZ designed the research study. CH and QW performed the research. HX and HH provided help and advice on the mechanical and RT-PCR experiments. JS analyzed the data. All authors contributed to editorial changes in the manuscript. All authors read and approved the final manuscript.

Ethics approval and consent to participate

All patients involved in this study gave their informed consent. Institutional review board approval of our hospital was obtained for this study (IRB file number: 2020-36).

Acknowledgment

We appreciate the kind help from Daniel Edward Porter and Whitney Annie Long in polishing this manuscript. Thanks to all reviewers for their opinions and suggestions.

Funding

This work was supported by the National Key Research and Development Program of China (2016YFA0101100),

National Natural Science Foundation of China (81930052), Tsinghua University Initiative Scientific Research Program (20161080069) and Pilot Fund of the The First Hospital of Tsinghua University (LH-03).

Conflict of interest

The authors declare no conflict of interest.

References

[1] Fishbein GA, Fishbein MC. Mitral Valve Pathology. Current Cardiology Reports. 2019; 21: 61.

[2] Spadaccio C, Mozetic P, Nappi F, Nenna A, Sutherland F, Trombetta M, *et al.* Cells and extracellular matrix interplay in cardiac valve disease: because age matters. Basic Research in Cardiology. 2016; 111: 16.

[3] Oyama MA, Elliott C, Loughran KA, Kossar AP, Castillero E, Levy RJ, *et al.* Comparative pathology of human and canine myxomatous mitral valve degeneration: 5HT and TGF-β mechanisms. Cardiovascular Pathology. 2019; 46: 107196.

[4] van Engeland NCA, Bertazzo S, Sarathchandra P, McCormack A, Bouten CVC, Yacoub MH, *et al.* Aortic calcified particles modulate valvular endothelial and interstitial cells. Cardiovascular Pathology. 2017; 28: 36–45.

[5] Neri T, Hiriart E, van Vliet PP, Faure E, Norris RA, Farhat B, *et al.* Human pre-valvular endocardial cells derived from pluripotent stem cells recapitulate cardiac pathophysiological valvulogenesis. Nature Communications. 2019; 10: 1929.

[6] Kruithof BPT, Paardekooper L, Hiemstra YL, Goumans MJ, Palmen M, Delgado V, *et al.* Stress-induced remodelling of the mitral valve: a model for leaflet thickening and superimposed tissue formation in mitral valve disease. Cardiovascular Research. 2019; 116: 931–943.

[7] Han RI, Clark CH, Black A, French A, Culshaw GJ, Kempson SA, *et al.* Morphological changes to endothelial and interstitial cells and to the extra-cellular matrix in canine myxomatous mitral valve disease (endocardiosis). Veterinary Journal. 2013; 197: 388–394.

[8] Ali MS, Deb N, Wang X, Rahman M, Christopher GF, Lacerda CMR. Correlation between valvular interstitial cell morphology and phenotypes: a novel way to detect activation. Tissue and Cell. 2018; 54: 38–46.

[9] Gonzalez Rodriguez A, Schroeder ME, Walker CJ, Anseth KS. FGF-2 inhibits contractile properties of valvular interstitial cell myofibroblasts encapsulated in 3D MMP-degradable hydrogels. APL Bioengineering. 2018; 2: 046104.

[10] Blomme B, Deroanne C, Hulin A, Lambert C, Defraigne J, Nusgens B, *et al.* Mechanical strain induces a pro-fibrotic phenotype in human mitral valvular interstitial cells through RhoC/ROCK/MRTF-a and Erk1/2 signaling pathways. Journal of Molecular and Cellular Cardiology. 2019; 135: 149–159.

[11] Morvan M, Arangalage D, Franck G, Perez F, Cattan-Levy L, Codogno I, *et al.* Relationship of Iron Deposition to Calcium Deposition in Human Aortic Valve Leaflets. Journal of the American College of Cardiology. 2018; 73: 1043–1054.

[12] Dekker S, van Geemen D, van den Bogaerdt AJ, Driessen-Mol A, Aikawa E, Smits AIPM. Sheep-Specific Immunohistochemical Panel for the Evaluation of Regenerative and Inflammatory Processes in Tissue-Engineered Heart Valves. Frontiers in Cardiovascular Medicine. 2018; 5: 105.

[13] Jabłońska-Trypuć A, Matejczyk M, Rosochacki S. Matrix metalloproteinases (MMPs), the main extracellular matrix (ECM) enzymes in collagen degradation, as a target for anticancer drugs. Journal of Enzyme Inhibition and Medicinal Chemistry. 2016; 31: 177–183.

[14] Rabkin SW. The Role Matrix Metalloproteinases in the Production of Aortic Aneurysm. Progress in Molecular Biology and Translational Science. 2017; 73: 239–265.

[15] Kuliczkowski W, Banaszkiewicz M, Mysiak A, Makaś G, Bil-Lula I. Does Arterial Hypertension Affect Plasma Levels of Matrix Metalloproteinases and their Tissue Inhibitors in Patients with Stable Coronary Artery Disease? A Preliminary Study. Cardiology Research and Practice. 2019; 2019: 1–8.

[16] Jackson HW, Defamie V, Waterhouse P, Khokha R. TIMPs: versatile extracellular regulators in cancer. Nature Reviews Cancer. 2017; 17: 38–53.

[17] Aloui S, Zidi W, Ouali S, Guizani I, Hadj-Taieb S, Mourali MS, *et al.* Association of matrix metalloproteinase 3 and endogenous inhibitors with inflammatory markers in mitral valve disease and calcification. Molecular Biology Reports. 2018; 45: 2135–2143.

[18] Mechmeche R, Zaroui A, Aloui S, Boukhris M, Allal-Elasmi M, Kaabachi N, *et al.* Late mitral restenosis after percutaneous commissurotomy: Predictive value of inflammation and extracellular matrix remodeling biomarkers. Heart & Lung. 2017; 46: 258–264.

[19] Dreger SA, Taylor PM, Allen SP, Yacoub MH. Profile and localization of matrix metalloproteinases (MMPs) and their tissue inhibitors (TIMPs) in human heart valves. Journal of Heart Valve Disease. 2002; 11: 875–880.

[20] Meador WD, Mathur M, Sugerman GP, Jazwiec T, Malinowski M, Bersi MR, *et al.* A Detailed Mechanical and Microstructural Analysis of Ovine Tricuspid Valve Leaflets. Acta Biomater. 2020; 102: 100–113.

[21] Karthik MK, Kaitlyn T, Toni W, Daniel PH, Frederick JS, Michael SS, *et al.* Biology and Biomechanics of the Heart Valve Extracellular Matrix. Review. Journal of Cardiovascular Development and Disease. 2020; 7: 57.